analytical chemistry

Article

Cite This: Anal. Chem. 2019, 91, 15317−15324

pubs.acs.org/ac

Binding-Induced 3D-Bipedal DNA Walker for Cascade Signal Amplification Detection of Thrombin Combined with Catalytic Hairpin Assembly Strategy

Erhu Xiong,[†] Deshuai Zhen,[‡,§] Ling Jiang,[*,§] and Xiaoming Zhou[*,†]

[†]School of Life Sciences, South China Normal University, Guangzhou 510631, China

[‡]College of Chemistry and Chemical Engineering, Qiannan Normal University for Nationalities, Duyun 558000, China

[§]State Key Laboratory of Chemo/Biosensing and Chemometrics, College of Chemistry and Chemical Engineering, Hunan University, Changsha 410082, China

Supporting Information

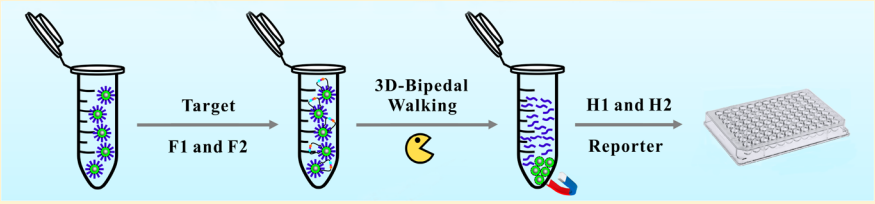

ABSTRACT: As an important biomarker, thrombin (TB) is a major player in thrombosis and hemostasis and has attracted increasing attention involving its determination. Herein a universal and ultrasensitive fluorescence biosensor based on a binding-induced 3D-bipedal DNA walker and catalytic hairpin assembly (CHA) strategy has been proposed for cascade signal amplification detection of thrombin. In this study, we designed two proximity probes (foot 1 and foot 2) which include a specific affinity ligand for TB binding and a Pb^{2+}-dependent DNAzyme tail sequence. In the presence of TB, the simultaneous binding of TB to foot 1 (F1) and foot 2 (F2) via TB aptamer (TBA) brings the tail sequences into close proximity and the melting temperature for tail sequences and track DNA is increased, allowing the Pb^{2+}-dependent DNAzyme to cleave the track DNA into two short fragments which have lower affinities for the DNAzyme and, finally, leading to the release of trigger DNA (T-DNA) for subsequent CHA reaction. In the meantime, the dissociated DNA walkers (F1 and F2) explore adjacent unwound track DNA, and the walking procedure is conducted. Unlike the conventional unipedal DNA walkers that anchor foot DNA and track DNA on the same sensing surface, the proposed 3D-bipedal DNA walking machine can not only increase the local concentration of track DNA but can also improve the walking efficiency and expand the range of the walkers to some extent due to the two free feet. Moreover, with the advantages of superior sensitivity and excellent specificity, this biosensing platform exhibits a huge potential in practical application in biomedical research and clinical diagnosis.

In most life activities, proteins play an important role, such as heredity, metabolism, and immunization.[1,2] The significant impacts have inspired researchers, and protein determination has received increasing attention for clinical diagnosis, food security, biomedical research, forensic analysis, and drug screening.[3−5] In the last few decades, nucleic acids have become very popular for the assembly of various nanostructures. Due to the well-defined Watson−Crick base pairing rules, excellent robustness, and universality, DNA is an important part of artificial DNA molecular machines.[6] Recently, various DNA molecular machines, for instance, DNA gears, switches, robots, walkers, and tweezers, have been developed on the basis of programmable and precise DNA molecule self-assembly using DNA as building blocks.[7−16] In particular, DNA walkers, as artificial nanomachines, have been extensively applied in biosensing platforms due to high-efficiency self-assembly nanostructures, cargo handling capabilities, and diverting biomimetic phenomena, enhancing the assay sensitivity and having huge potential in biomedical research.[17−19] Upon these motions, DNA walkers can generate copious signal molecules for signal amplification along multidimensional tracks.[20−23] For instance, Chen et al. proposed an electrochemical biosensing platform for an anti-digoxigenin antibody assay based on proximity recognition and a polymerase-driven DNA walker.[24] Wang et al. developed a signal-enhanced fluorescent DNA walker on DNA origami for nucleic acid detection.[25] However, due to the inadequate walking space of one-dimensional (1D) DNA footpaths[26−28] or two-dimensional (2D) DNA origami[25,29,30] and low fluxes of the substrate probe in nanostructures, in recent years, there has been an increasing interest in three-dimensional (3D) tracks, which are built on the surface of micro- or nanoparticles and have a strong DNA loading capability, strikingly enhancing the concentration of local probes on the surface for higher

Received: November 1, 2019
Accepted: November 11, 2019
Published: November 11, 2019

DOI: 10.1021/acs.analchem.9b04987
Anal. Chem. 2019, 91, 15317−15324

Scheme 1. TB Detection Based on Binding-Induced 3D-Bipedal Walking and CHA Strategy

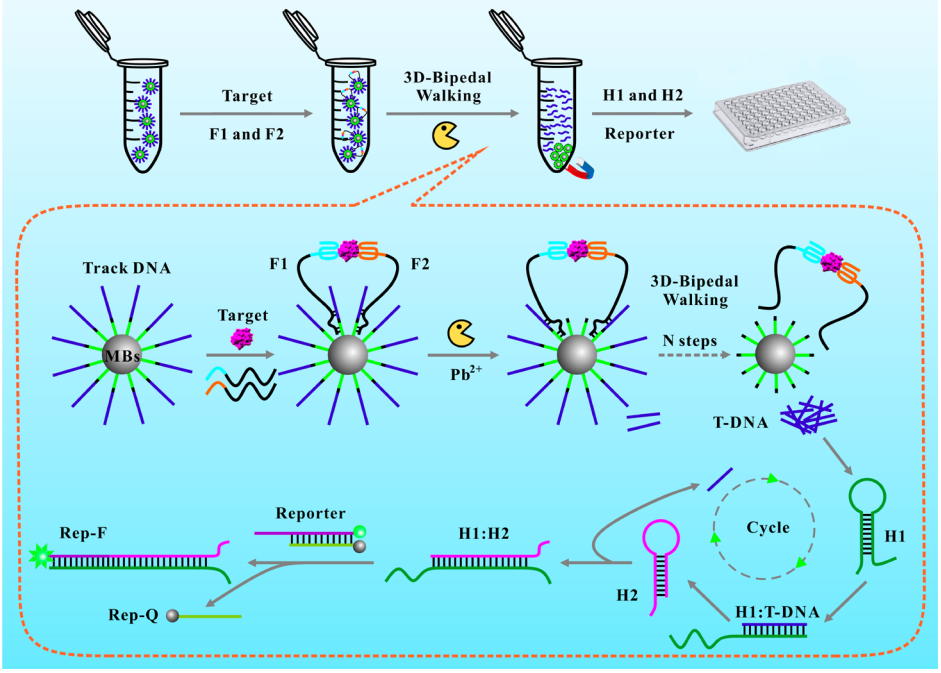

walking efficiency and better signal amplification efficiency owing to the large specific surface area of micro- or nanoparticles. For instance, Li and co-workers reported a dual-enzyme-mediated 3D-DNA walker by employing T4 polynucleotide kinase as catalysts and application for polynucleotide kinase detection.[31] Liao and co-workers proposed an electrochemiluminescence biosensing platform for the ultrasensitive assay of laminin on the basis of DNA dendrimer-carried luminophore and DNA nanomachine-assisted target recycling amplification.[32] Although these 3D-DNA unipedal walkers have achieved satisfying sensitivity, they are generally related to the adoption of one or more protein enzymes to drive the automatic motions of DNA walkers, which limits their extensive applications. As we know, protein enzymes are impressionable to some experimental conditions, such as pH, temperature, humidity, and ionic concentration, which readily cause low detection sensitivity and reproducibility.[33−35] To address these issues, researchers adopted metal ion-dependent DNAzymes as the driving force of the DNA walker due to their outstanding catalytic activity, intrinsic signal amplification acquired by high thermal stability, multiple enzymatic turnovers, and better economics compared with their counterpart protein enzymes. Additionally, it is easy to control the DNAzyme activity by regulating the depletion or addition of the cofactor metal ions, which can switch the DNA walker off or on. In view of this advantage, Zhang et al. proposed a target-induced Mg^{2+}-dependent DNAzyme machine for signal amplification determination of thrombin (TB) with a detection limit of 5 pM.[36] Kong and co-workers developed a biostable, highly integrated, and Mn^{2+}-dependent DNAzyme-powered DNA machine which could operate in vivo.[37] Even though the metal ion-dependent DNAzymes can be applied to drive the motion of 3D-DNA walkers, the reported DNA walkers mentioned above have one foot assembled on the surface of nanoparticles, which will limit the movement range and efficiency of the DNA walking machines. In addition, the fabrication of two sorts of DNA probes (track DNA and foot DNA) on the same micro- or nanoparticle surface can decrease the local concentration of track DNA for signal amplification due to the occupation of foot DNA and increase the difficulty of the assembly of multiple DNA probes with different concentration ratios. At present, to solve this problem, Li et al. dexterously developed a bipedal DNA walker for electrochemical detection of several proteins, which only needed to assemble one kind of DNA strand on the biosensing surface.[38] Subsequently, based on this principle, Miao et al. reported a bipedal DNA walker-based electrochemical biosensing platform for target DNA assay with good analytical performance.[39] Although, this kind of bipedal DNA walker based on metal ion-dependent DNAzymes can provide a novel approach for target detection, the use of 1D-DNA footpaths restrict the further improvement of sensitivity. Therefore, it is indeed necessary to develop DNAzyme-based 3D-bipedal DNA walkers for target assay.

In addition to the 3D-bipedal DNA walking strategy, the cascade signal amplification method is another important method for amplified target detection. To achieve outstanding analysis capability, multiple signal amplification methods are combined. Due to the programmability and high signal-to-noise ratio, the catalytic hairpin assembly (CHA) strategy has been widely employed for varied biosensing systems and can be considered as a new generation of nonenzymatic signal amplifiers and transducers, which can yield stable double-stranded DNA nanostructures as a result of an initiation of a single-stranded catalyst and can obtain a 50- to 100-fold signal amplification within a few hours.[34,40−45] However, as far as we know, a protein binding-induced 3D-bipedal DNA walker for amplified protein detection has rarely been reported. Therefore, the development of a 3D-bipedal DNA walker for protein assay with reliable, convenient, enzyme-free, and cost-effective attributes would be highly desirable, which will directly improve sensitivity and specificity.

Herein, taking into account the advantages of 3D pattern (large specific surface area with high DNA loading capability),

DOI: 10.1021/acs.analchem.9b04987
Anal. Chem. 2019, 91, 15317−15324

bipedal DNA walker (higher walking range and efficiency), metal ion-dependent DNAzyme (high thermal stability, multiple enzymatic turnovers, and better economics), and CHA reaction (programmability, high signal-to-noise ratio, and nonenzymatic signal amplifier), we developed a protein binding-induced 3D-bipedal DNA walker for cascade-amplified protein assay. Unlike the conventional unipedal DNA molecular machines, the developed DNA walker device has triple amplification containing metal ion-dependent DNAzyme-based bipedal DNA walking, magnetic enrichment, and CHA. The specific principle of the work is shown in Scheme 1. First, we designed two proximity probes (foot 1 and foot 2) which include a specific affinity ligand for the target protein (here we selected TB, the central protease in the blood coagulation cascade proteases, as the target analyte of interest.[46,47]) binding and a Pb^{2+}-dependent DNAzyme tail sequence. In the absence of TB, single foot 1 (F1) or foot 2 (F2) cannot hybridize with track DNA because the complementary fragments are too short to facilitate efficient hybridization owing to the low melting temperature (T_m < 25 °C).[38,48,49] However, in the presence of TB, the binding of TB to the F1 and F2 simultaneously via TB aptamer (TBA) brings the tail sequences into close proximity and the melting temperature for tail sequences and track DNA is increased, allowing the Pb^{2+}-dependent DNAzyme to cleave the track DNA into two short fragments which have lower affinities for the DNAzyme and, finally, leading to the release of trigger DNA (T-DNA) for subsequent CHA reaction. In the meantime, the dissociated DNA walkers (F1 and F2) explore adjacent unwound track DNA and the walking procedure is conducted. Due to the wide 3D walking range, high local concentration of track DNA, and effective bipedal DNA walking, the proposed 3D-bipedal DNA walker results in an amazing amplification effect by generating copious T-DNA for subsequent CHA reaction. After magnetic separation and transition to CHA system, the T-DNA unfolds hairpin 1 (H1) because of the hybridization between the complementary sequences on the T-DNA and H1. Next, the unclosed H1 hybridizes with hairpin 2 (H2) to displace the T-DNA and to form the H1/H2 complex. The displaced T-DNA can initiate the next cycle of the CHA reaction, leading to the yield of copious H1/H2 complexes which serve as an initiator of the fluorescent reporter to yield amplified fluorescent signal. Based on the above protein binding-induced 3D-bipedal DNA walker and CHA amplification strategy, the proposed fluorescent biosensing platform has been successfully used for TB determination and shows superior analytical performance with the limit of detection as low as 23 fM. Furthermore, the biosensor exhibits a good selectivity and applicability in serum samples. Therefore, the proposed method may supply a robust and sensitive biosensing platform for selective assay of other biomarkers.

EXPERIMENTAL SECTION

Materials. All oligonucleotides (Table S1) used in this work, 40% acrylamide/bis solution (19:1), ethylenediaminetetraacetic acid (EDTA), and 10× Tris-borate-EDTA (TBE) buffer were supplied by Sangon Biotech Co., Ltd. (Shanghai, China). Streptavidin-coated Dynabeads M-270 (2.8 μm, catalog no. 65305) were purchased from Invitrogen (ThermoFisher Scientific, Shanghai, China). A 6× gel loading dye was obtained from New England Biolabs Inc. (Beijing, China). SYBR Gold was obtained from Life Technologies (Guangzhou, China). TEMED, ammonium persulfate (APS), thrombin (TB), bovine serum albumin (BSA), carcinoembryonic antigen (CEA), alpha fetoprotein (AFP), immunoglobulin G (IgG), urea, human serum, HEPES, KCl, tris base, dimethyl sulfoxide (DMSO), $MgCl_2$, Triton X-100, and NaCl were supplied by Sigma-Aldrich Inc. (Shanghai, China) and used without further purification. Ultrapure water obtained from a Millipore water purification system (≥18 MΩ cm, Milli-Q, Millipore) was used in all assays.

Apparatus. Eppendorf Mastercycler Nexus GX2 (Shanghai, China), LightCylcer 96 Plate Reader (Roche, Shanghai, China), and Nunc 96-well Plate (Yubo Biotech Company, Shanghai, China) were used. A ChemiDoc MP Imaging System (Bio-Rad Laboratories Inc., Shanghai, China) was used. An Invitrogen DYNAL magnet (ThermoFishers Scientific, Shanghai, China) was used.

Magnetic Bead Washing and Immobilization of Track DNA. First, the streptavidin-coated magnetic bead (MB) slurry was shocked to homogeneity before dispensing. Then 20 μL (10 mg/mL) of streptavidin-coated MBs was transferred into a 1.5 mL EP tube and suspended in 500 μL of 10 mM Tris-HCl buffer (1 mM EDTA, 2 M NaCl, pH 7.5). After that, the EP tube was placed on a magnet for 2 min, and then the supernatant was discarded. The streptavidin-coated MBs were resuspended in 500 μL of 10 mM Tris-HCl buffer. The above step was repeated three times, and the washed MBs were resuspended in 50 μL of the same buffer including 10 μM the biotinylated track DNA. Then the mixture was incubated at 25 °C for 15 min with gentle rotation to enable streptavidin−biotin interaction (K_d = 10^{-15} M). The biotinylated track DNA-coated MBs were separated with a magnet for 2 min and then resuspended in 500 μL of 10 mM Tris-HCl buffer. This step was repeated three times, and the biotinylated track DNA-coated MBs were resuspended in 30 μL of 25 mM HEPES buffer (20 mM KCl, 150 mM NaCl, 1% DMSO, and 0.05% Triton X-100, pH 7.5).

Native Polyacrylamide Gel Electrophoresis Analysis. To verify whether the designed sequences led to the desired reaction pathways, a polyacrylamide gel electrophoresis (PAGE)-based analysis was performed that can confirm the existence of reaction pathways. A total of 10 mL of PAGE premix was first prepared containing 10 μL of TEMED, 110 μL of 10% APS, 2.5 mL of 40% acrylamide and bis(acrylamide) solution (19:1), 1 mL of 10× TBE buffer, and 6.38 mL of deionized water. After the preparation of 10% native PAGE, the gel was prerun at 180 V for 30 min. Subsequently, samples with 1× gel loading dye were added into the wells, and the gel was run at 130 V for 1 h. Finally, the gel was stained for 15 min in SYBR Gold dye solution and photographed by the gel imaging system.

Real-Time Fluorescence Analysis of TB. Prior to the amplification reaction, 50 μL of 2.5 μM H1, 50 μL of 5 μM H2, and 50 μL of 2.5 μM Reporter (2.5 μM Rep-F and 3 μM Rep-Q) were heated to 90 °C for 5 min and then slowly cooled to 25 °C at a rate of 0.1 °C·s^{-1} in 25 mM HEPES buffer (20 mM KCl, 150 mM NaCl, pH 7.5), respectively. The 3D-bipedal walking amplification reaction was executed in 50 μL of reaction solution including 30 μL of biotinylated track DNA-coated MBs, 2.5 μL of 10 μM F1, 2.5 μL of 10 μM F2, 5 μL of 1 mM Pb^{2+}, 9 μL of 1× HEPES buffer, and 1 μL of TB with various concentrations. After incubation of the above mixture at 37 °C with gentle rotation for 1.5 h, the supernatant was separated with a magnet for 2 min and the supernatant was

DOI: 10.1021/acs.analchem.9b04987
Anal. Chem. 2019, 91, 15317−15324

transferred into a 96-well plate with the addition of 2.5 μM H1, 5 μM H2, and 2.5 μM Reporter, which was immediately transferred to a plate reader for fluorescence measurements at 37 °C for 3 h with an excitation wavelength of 485 nm and emission wavelength of 528 nm.

RESULTS AND DISCUSSION

Feasibility of the Developed Biosensor for TB Detection. To evaluate the feasibility of the proposed biosensing platform, fluorescence analysis was performed. As shown in Figure 1A, there was no obvious fluorescence signal

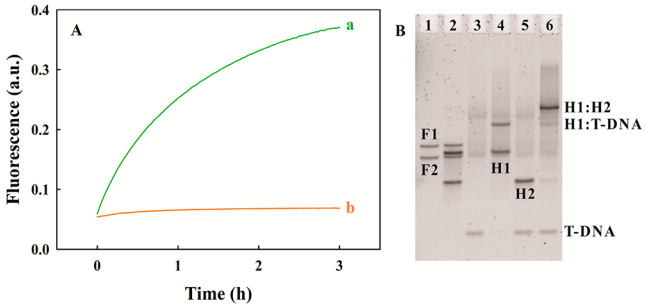

Figure 1. Feasibility of the proposed biosensing platform. (A) Fluorescence responses of the biosensing system in the presence of 0.5 nM TB (curve a) and in absence of TB (curve b). (B) 10% native PAGE to analyze the proposed biosensing platform. Lane 1: supernatant (F1+F2+without TB), lane 2: supernatant (F1+F2+without TB)+H1+H2, lane 3: supernatant (F1+F2+with TB), lane 4: supernatant (F1+F2+with TB)+H1, lane 5: supernatant (F1+F2+with TB)+H2, lane 6: supernatant (F1+F2+with TB)+H1+H2. 0.5 μM F1, 0.5 μM F2, 2.5 μM H1, and 5 μM H2 were used in the electrophoresis analysis.

in the absence of TB (curve a). Nevertheless, in the presence of 0.5 nM TB, a significant fluorescence signal was obtained, which should contribute to the 3D-bipedal walking amplification reaction and CHA reaction (curve b). Furthermore, the amplification reaction was also verified by the 10% native PAGE image. As displayed in Figure 1B, lane 1 represents the bands of F1 and F2. Lane 2 shows the bands of F1, F2, H1, and H2. Lane 3 is the band of supernatant after separation with a magnet, and a band of T-DNA was observed, indicating that the 3D-bipedal walking amplification reaction had occurred in the presence of TB and that copious T-DNA was released. After mixing H1 with the supernatant, the band of T-DNA disappeared and a new band of H1:T-DNA duplex appeared, demonstrating that the released T-DNA in the supernatant can unfold the H1 to form H1:T-DNA duplex. In lane 5, after mixing H2 with the supernatant, the band of T-DNA was still observed and no new band appeared, demonstrating that there is no interaction between H2 and T-DNA. However, after the addition of H1 and H2 into the supernatant, as displayed in lane 6, there was an obvious new band of H1:H2 duplex compared with lane 5 due to the CHA reaction, and the band of T-DNA was still observed because of the recycling. All of the above results indicated that the proposed biosensor based on the protein binding-induced 3D-bipedal DNA walker and CHA amplification strategy was feasible for amplified and sensitive detection of TB.

Optimization of Experimental Conditions for the Developed Biosensor. A critical conception to our success in the present work is the cleavage induced by TB binding to accelerate 3D-bipedal walking in the presence of TB and minimized without TB binding. Some crucial experimental parameters, such as the length of proximity feet, reaction temperature, Pb^{2+} concentration, and reaction time, may play vital roles in commanding the whole reaction rate and potentially affect the final analytical capability of the biosensor. Therefore, these important experimental parameters should be optimized. First, as shown in Figure 2A, the proximity feet include a TBA, poly-T spacer, recognition ligand, and DNAzyme tails. In the present research, the 3′ side of the DNAzyme tail is anchored via five bases, and the 5′ side ranges from five bases to nine bases. Ideally, a shorter DNAzyme tail can reduce nonspecific cleavage to a great extent; nevertheless, a too short DNAzyme tail can make it difficult to achieve specific signal strength, while a strong false positive signal will be generated due to an overlength of DNA duplex. As shown in Figure 2B, with the increase of complementary base number of the 5′ side of the DNAzyme tail, the initial rate in the presence of 50 pM TB gradually increases (purple bars), whereas the background signal also increases even in the absence of TB (green bars). Although the initial rates are pretty high for the DNAzyme tail with eight and nine bases, their signal-to-noise ratios are very low. Thus, we selected the DNAzyme tail with seven bases in this study.

Furthermore, the parameters of reaction temperature and Pb^{2+} concentration are also very important to the 3D-bipedal walking reaction, which may directly influence the kinetics of strand hybridization and the cleavage efficiency of DNAzyme. As shown in Figure 2C, the initial rates increase with the augment of temperature from 25 °C to 37 °C and decrease at 45 °C because the high temperature was not conducive to the toehold binding. Therefore, 37 °C was used in all experiments. As displayed in Figure 2D, the initial rates increase with the augment of Pb^{2+} concentration and reach a plateau after 100 μM; thus, 100 μM Pb^{2+} was selected as the optimized Pb^{2+} concentration. In addition, the reaction time is another key parameter for the biosensing analytical performance. As exhibited in Figure 2E, the values of the initial rate increase rapidly with the increase of reaction time and reach a plateau after 1.5 h, so 1.5 h was chosen as the optimal reaction time.

Comparison of Walking Efficiency between Bipedal and Unipedal Walkers. To compare the walking efficiency of the two different kinds of DNA walker, a 3D-unipedal walking method was designed. As shown in Scheme S1, Bio-TBA strand and track DNA were assembled on the MB surface in a proper ratio. In the presence of TB, the binding of TB to the Bio-TBA and F strand simultaneously brings the tail sequence of F strand into close proximity, allowing the Pb^{2+}-dependent DNAzyme to cleave the track DNA into two short fragments which have lower affinities for the DNAzyme and, finally, resulting in the release of T-DNA for subsequent CHA reaction. To keep the 3D-unipedal walking system in optimal condition and achieve optimum analytical performance, the concentration ratio of track DNA/Bio-TBA was investigated. The concentration ratio was adjusted from 5 to 40, as displayed in Figure 3A, and the initial rates increase with the augment of concentration ratio and reach the maximum at a ratio of 20. When the concentration ratio further increases to 40, the initial rate decreases due to the insufficient assembly of Bio-TBA for the binding of TB and F strand. Therefore, the track DNA with 20-fold concentration more than that of Bio-TBA was selected in the 3D-unipedal walking system. After obtaining the optimal experimental condition, we evaluated the

DOI: 10.1021/acs.analchem.9b04987
Anal. Chem. 2019, 91, 15317−15324

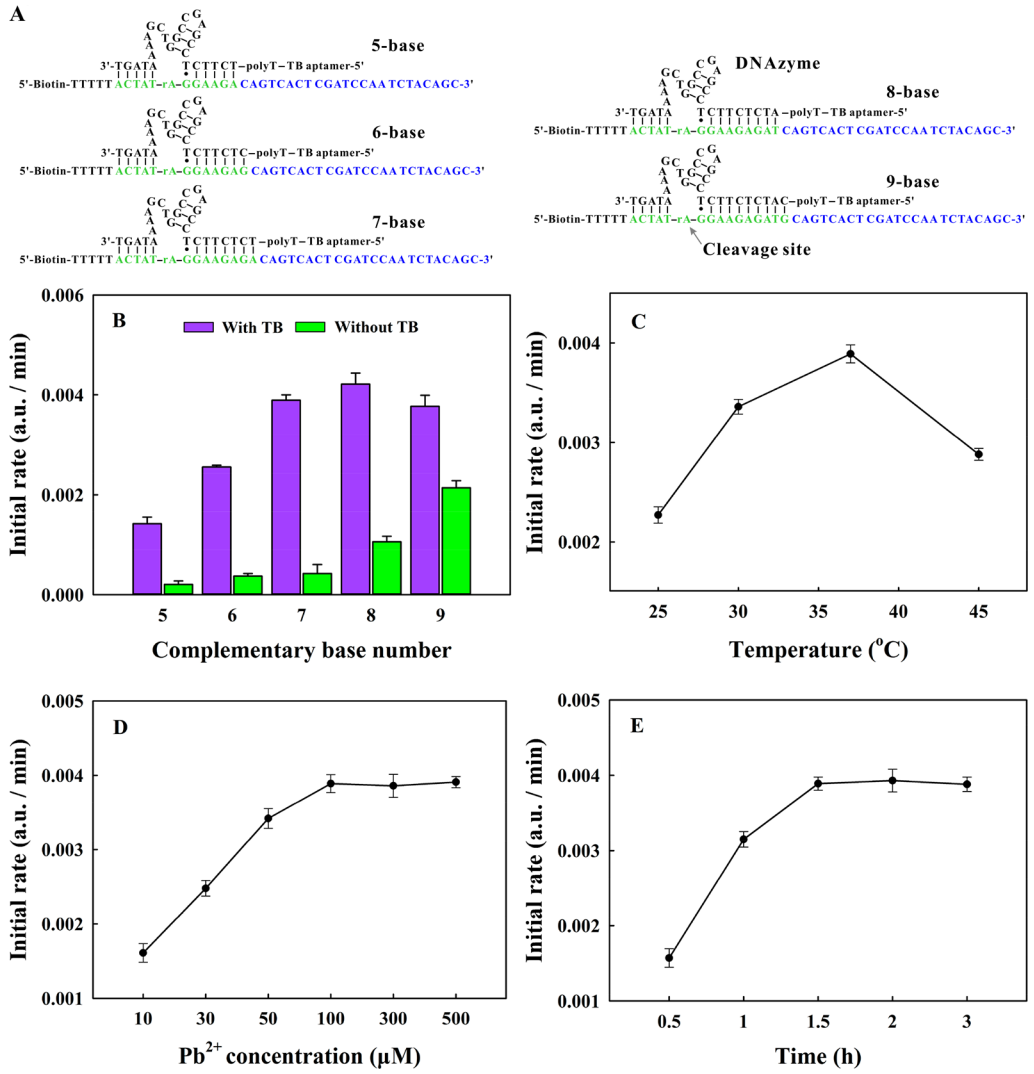

Figure 2. Optimization of experimental conditions for the developed biosensor. (A) Five kinds of designed proximity probes and the relevant track DNA. (B) The values of initial rate with different lengths (five, six, seven, eight, and nine bases) of the 5′ side of the DNAzyme tails. The green bars are the values of initial rate of background responses, while the purple bars are the values of initial rate in the presence of 50 pM TB. (C) Effects of reaction temperature. (D) Effects of Pb^{2+} concentration. (E) Effects of reaction time. TB concentration: 50 pM. Error bars represent the standard deviation of three individual experiments.

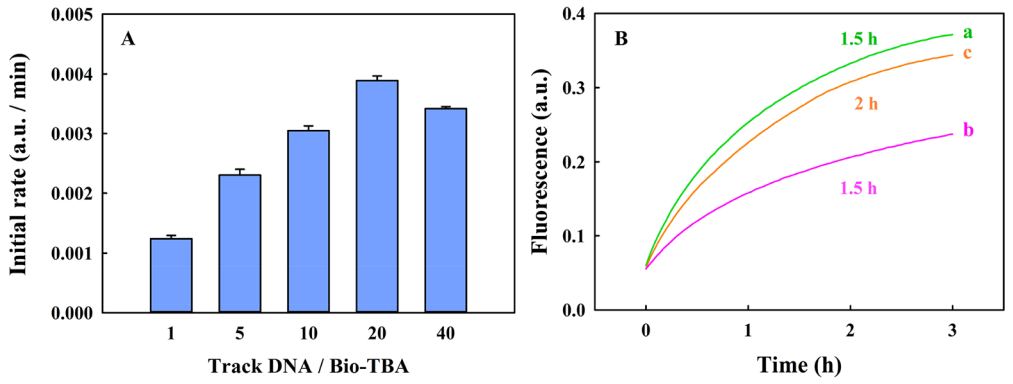

Figure 3. (A) Optimization of the concentration ratio of track DNA/Bio-TBA. (B) Fluorescence responses of the bipedal walker and unipedal walker.

walking efficiency of the two different walkers in the presence of 0.5 nM TB. As shown in Figure 3B, after incubation for 1.5 h, the reaction rate of the unipedal walking system (curve b) was much slower than that of the bipedal walking system (curve a). When the incubation time of the unipedal walking system was increased to 2 h, its reaction rate (curve c) increased and was only a little smaller than that of bipedal walking system (curve a). These above results clearly indicated

DOI: 10.1021/acs.analchem.9b04987
Anal. Chem. 2019, 91, 15317−15324

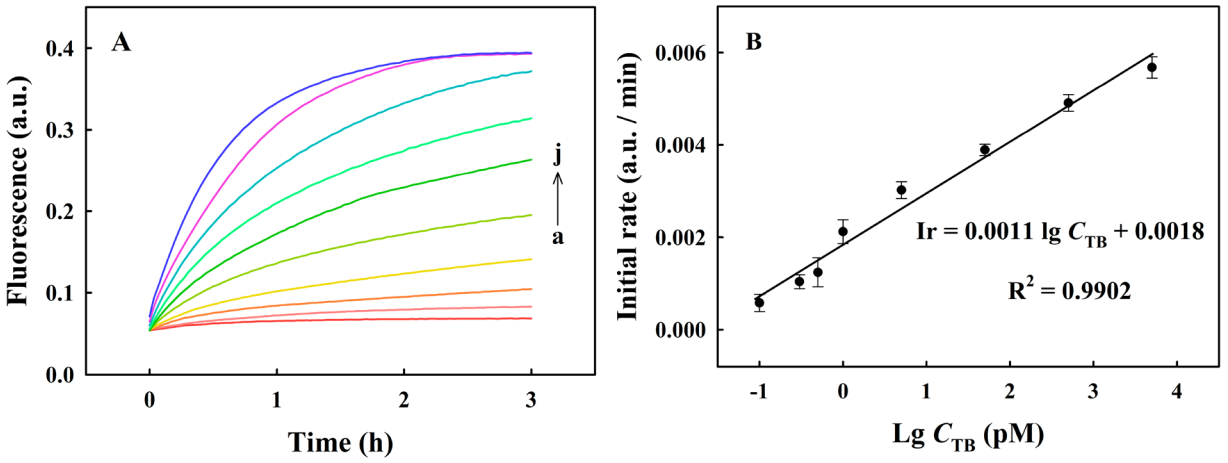

Figure 4. (A) Fluorescence responses of the biosensing system upon the addition of TB with different concentrations (a to j: 0 pM, 0.1 pM,0.3 pM, 0.5 pM, 1 pM, 5 pM, 50 pM, 500 pM, 5 nM, 10 nM). (B) The linear relationship between the initial rate and the logarithm of TB concentration. Error bars represent the standard deviation of three individual experiments.

that the walking efficiency of the proposed 3D-bipedal walker was much higher than that of the conventional unipedal DNA walkers.

Analytical Performance. Under optimal experimental conditions, the proposed biosensor based on protein binding-induced 3D-bipedal DNA walker and CHA amplification strategy was evaluated with varied TB concentrations. As exhibited in Figure 4A, the fluorescence signals are enhanced with the augment of TB concentrations ranging from 0.1 pM to 10 nM. Furthermore, it is worth noting that the initial rate is linear with the logarithm of TB concentrations ranging from 0.1 pM to 5 nM. As exhibited in Figure 4B, the linear regression equation is Ir = 0.0011 lg C_{TB} + 0.0018 (R^2 = 0.9902, Ir represents the initial rate) with a detection limit of 23 fM (S/N = 3), indicating that the proposed biosensing platform has a superior analysis capability compared with that of some reported analytical technologies (Table S2) and conventional unipedal DNA walking biosensors for TB detection (Table S3).

Specificity and Practical Application of the Developed Biosensor. Specificity is a key factor for investigating the success of the developed biosensing platform. Therefore, to determine the specificity of the biosensing platform, a series of comparative studies between the TB and other proteins (BSA, CEA, AFP, and IgG) was carried out by measuring the fluorescence responses. As shown in Figure 5, the initial rates of 10 nM BSA, CEA, AFP, and IgG are almost as low as the blank value, respectively. In the presence of 50 pM TB, the initial rate is pretty high, and there is no obvious change in the initial rate when mixing them together, indicating that the proposed biosensing platform has a satisfactory specificity.

In addition, to investigate the practical application of the proposed biosensing platform for real samples, we added TB at various concentrations (5 nM, 50 pM, and 0.5 pM) to 10-fold diluted serum samples. As shown in Table 1, the recoveries for TB detection were 101.2%, 98.46%, and 104%, respectively, indicating that the developed biosensing platform has excellent anti-interference ability and is desirable for sensitive assays carried out in relatively complex biological samples.

CONCLUSION

In short, this study proposed a cascade signal amplification biosensing platform based on a protein binding-induced 3D-bipedal DNA walker and CHA amplification strategy. As we know, for the conventional unipedal DNA walkers that anchor the foot DNA and track DNA on the same sensing surface, the fabrication of two sorts of DNA probes not only reduces the local concentration of the track DNA owing to the occupation of foot DNA but also increases the difficulty of biosensor assembly of multiple DNA probes with different concentration ratios, while the proposed 3D-bipedal DNA walking machine in this work can increase the local concentration of track DNA, improve the walking efficiency, and expand the range of the walkers to some extent due to the two free feet. Moreover, the biosensing system also has some considerable advantages, such as good selectivity, enzyme-free, and a lower detection limit of

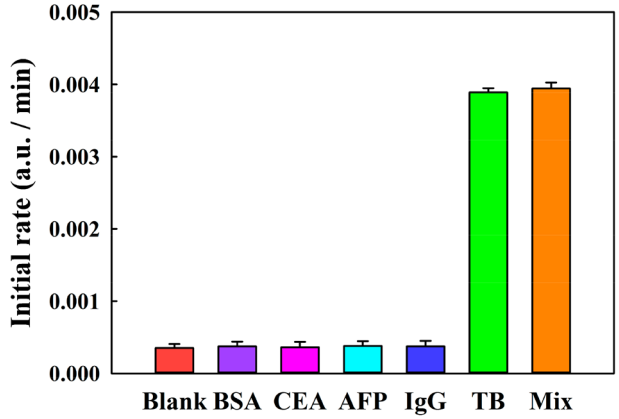

Figure 5. Comparison of the initial rate of the proposed biosensing platform in the absence of TB and in the presence of 50 pM TB, 10 nM BSA, 10 nM CEA, 10 nM AFP, and 10 nM IgG, respectively. Error bars represent the standard deviation of three individual experiments.

Table 1. Recovery Tests of TB Detection in 10-Fold Diluted Human Serum Samples[a]

sample no.	added	found	recovery (%)
1	5 nM	5.06 ± 0.42 nM	101.2
2	50 pM	49.23 ± 0.96 pM	98.46
3	0.5 pM	0.52 ± 0.07 pM	104

[a] n = 3, n stands for the number of individual experiments.

DOI: 10.1021/acs.analchem.9b04987
Anal. Chem. 2019, 91, 15317−15324

23 fM (S/N = 3). More importantly, it forsakes the cumbersome and expensive thermal cycling protocol, endowing the developed biosensing system with easy use and cost-efficiency in practical applications. Furthermore, it can be easily extended for detection of a variety of target proteins just through changing the corresponding aptamer sequences of the feet. Therefore, the proposed biosensing system has potential applications in biomedical research and clinical diagnosis.

■ ASSOCIATED CONTENT

Supporting Information

The Supporting Information is available free of charge on the ACS Publications website at DOI: 10.1021/acs.analchem.9b04987.

Sequences of all oligonucleotides used in this work, schematic illustration of TB detection based on binding-induced 3D-unipedal walking and CHA strategy, comparison of various analytical technologies for TB determination, and comparison of the analytical performance between bipedal DNA walker and unipedal DNA walker for TB determination (PDF)

■ AUTHOR INFORMATION

Corresponding Authors

*E-mail: ljiang630@163.com.
*E-mail: zhouxm@scnu.edu.cn.

ORCID

Xiaoming Zhou: 0000-0001-5597-4804

Notes

The authors declare no competing financial interest.

■ ACKNOWLEDGMENTS

This work was financially supported by National Natural Science Foundation of China (grants: 21904042, 21475048, 21874049).

■ REFERENCES

(1) van der Vaart, A.; Bursulaya, B. D.; Brooks, C. L.; Merz, K. M. *J. Phys. Chem. B* **2000**, *104*, 9554−9563.
(2) Li, N. X.; Du, M. Y.; Liu, Y. C.; Ji, X. H.; He, Z. K. *ACS Sensors* **2018**, *3*, 1283−1290.
(3) Li, G. X.; Yu, X. X.; Liu, D. Q.; Liu, X. Y.; Li, F.; Cui, H. *Anal. Chem.* **2015**, *87*, 10976−10981.
(4) Li, F.; Zhang, H. Q.; Lai, C.; Li, X. F.; Le, X. C. *Angew. Chem., Int. Ed.* **2012**, *51*, 9317−9320.
(5) Li, Y. H.; Zhao, Y. R.; Chan, W. H.; Wang, Y. J.; You, Q. H.; Liu, C. H.; Zheng, J.; Li, J. S.; Yang, S.; Yang, R. H. *Anal. Chem.* **2015**, *87*, 584−591.
(6) Shin, J. S.; Pierce, N. A. *J. Am. Chem. Soc.* **2004**, *126*, 10834−10835.
(7) Wilner, O. I.; Willner, I. *Chem. Rev.* **2012**, *112*, 2528−2556.
(8) Muscat, R. A.; Bath, J.; Turberfield, A. J. *Nano Lett.* **2011**, *11*, 982−987.
(9) Thubagere, A. J.; Li, W.; Johnson, R. F.; Chen, Z.; Doroudi, S.; Lee, Y. L.; Izatt, G.; Wittman, S.; Srinivas, N.; Woods, D.; et al. *Science* **2017**, *357*, eaan6558.
(10) Yang, Y. J.; Huang, J.; Yang, X. H.; Quan, K.; Wang, H.; Ying, L.; Xie, N. L.; Ou, M.; Wang, K. M. *Anal. Chem.* **2016**, *88*, 5981−5987.
(11) Liu, M. H.; Fu, J. L.; Hejesen, C.; Yang, Y. H.; Woodbury, N. W.; Gothelf, K.; Liu, Y.; Yan, H. *Nat. Commun.* **2013**, *4*, 2127.
(12) Cha, T. G.; Pan, J.; Chen, H. R.; Salgado, J.; Li, X.; Mao, C. D.; Choi, J. H. *Nat. Nanotechnol.* **2014**, *9*, 39−43.
(13) Amir, Y.; Ben Ishay, E.; Levner, D.; Ittah, S.; Abu Horowitz, A.; Bachelet, I. *Nat. Nanotechnol.* **2014**, *9*, 353−357.
(14) Wang, F. A.; Liu, X. Q.; Willner, I. *Angew. Chem., Int. Ed.* **2015**, *54*, 1098−1129.
(15) Wei, B.; Yao, D. B.; Zheng, B.; Zhou, X.; Guo, Y. J.; Li, X.; Li, C. X.; Xiao, S. Y.; Liang, H. J. *ACS Appl. Mater. Interfaces* **2019**, *11*, 19724−19733.
(16) Yang, Y. J.; Huang, J.; Yang, X. H.; He, X. X.; Quan, K.; Xie, N. L.; Ou, M.; Wang, K. M. *Anal. Chem.* **2017**, *89*, 5850−5856.
(17) Li, Y. Y.; Wang, G. A.; Mason, S. D.; Yang, X. L.; Yu, Z. C.; Tang, Y. Y.; Li, F. *Chem. Sci.* **2018**, *9*, 6434−6439.
(18) Ma, P. Q.; Liang, C. P.; Zhang, H. H.; Yin, B. C.; Ye, B. C. *Chem. Sci.* **2018**, *9*, 3299−3304.
(19) Liu, W.; Chen, A. Y.; Li, S. K.; Peng, K. F.; Chai, Y. Q.; Yuan, R. *Anal. Chem.* **2019**, *91*, 1516−1523.
(20) Mendoza, O.; Mergny, J. L.; Aimé, J. P.; Elezgaray, J. *Nano Lett.* **2016**, *16*, 624−628.
(21) Yang, X. L.; Tang, Y. N.; Mason, S. D.; Chen, J. B.; Li, F. *ACS Nano* **2016**, *10*, 2324−2330.
(22) He, M. Q.; Wang, K.; Wang, W. J.; Yu, Y. L.; Wang, J. H. *Anal. Chem.* **2017**, *89*, 9292−9298.
(23) Li, W.; Wang, L.; Jiang, W. *Chem. Commun.* **2017**, *53*, 5527−5530.
(24) Chen, Z. Q.; Wang, C.; Hao, L. J.; Gao, R.; Li, F.; Liu, S. F. *Biosens. Bioelectron.* **2019**, *128*, 104−112.
(25) Wang, D. F.; Vietz, C.; Schröder, T.; Acuna, G.; Lalkens, B.; Tinnefeld, P. *Nano Lett.* **2017**, *17*, 5368−5374.
(26) He, Y.; Liu, D. R. *Nat. Nanotechnol.* **2010**, *5*, 778−782.
(27) Liu, M. H.; Cheng, J.; Tee, S. R.; Sreelatha, S.; Loh, I. Y.; Wang, Z. S. *ACS Nano* **2016**, *10*, 5882−5890.
(28) Peng, L. C.; Zhang, P.; Chai, Y. Q.; Yuan, R. *Anal. Chem.* **2017**, *89*, 5036−5042.
(29) Tomov, T. E.; Tsukanov, R.; Glick, Y.; Berger, Y.; Liber, M.; Avrahami, D.; Gerber, D.; Nir, E. *ACS Nano* **2017**, *11*, 4002−4008.
(30) Yang, Y. Y.; Goetzfried, M. A.; Hidaka, K.; You, M. X.; Tan, W. H.; Sugiyama, H.; Endo, M. *Nano Lett.* **2015**, *15*, 6672−6676.
(31) Feng, C.; Wang, Z. H.; Chen, T. S.; Chen, X. X.; Mao, D. S.; Zhao, J.; Li, G. X. *Anal. Chem.* **2018**, *90*, 2810−2815.
(32) Li, L.; Niu, C. C.; Li, T.; Wan, Y. F.; Zhou, Y.; Wang, H. J.; Yuan, R.; Liao, P. *Biosens. Bioelectron.* **2018**, *101*, 206−212.
(33) Zhang, J.; Wang, L. L.; Hou, M. F.; Xia, Y. K.; He, W. H.; Yan, A.; Weng, Y. P.; Zeng, L. P.; Chen, J. H. *Biosens. Bioelectron.* **2018**, *102*, 33−40.
(34) Wang, R.; Wang, L.; Xu, X. W.; Jiang, W. *Sens. Actuators, B* **2018**, *268*, 287−292.
(35) Xiong, E. H.; Zhen, D. S.; Jiang, L. *Talanta* **2019**, *198*, 179−184.
(36) Chen, J. B.; Zuehlke, A.; Deng, B.; Peng, H. Y.; Hou, X. D.; Zhang, H. Q. *Anal. Chem.* **2017**, *89*, 12888−12895.
(37) Wang, J.; Wang, D. X.; Tang, A. N.; Kong, D. M. *Anal. Chem.* **2019**, *91*, 5244−5251.
(38) Li, C.; Li, X. X.; Wei, L. M.; Liu, M. Y.; Chen, Y. Y.; Li, G. X. *Chem. Sci.* **2015**, *6*, 4311−4317.
(39) Chai, H.; Miao, P. *Anal. Chem.* **2019**, *91*, 4953−4957.
(40) Wang, M. W.; Tang, Y. Y.; Chen, Y. Y.; Cao, Y.; Chen, G. F. *Anal. Chim. Acta* **2019**, *1045*, 77−84.
(41) Chang, C. C.; Chen, C. P.; Chen, C. Y.; Lin, C. W. *Chem. Commun.* **2016**, *52*, 4167−4170.
(42) Zhu, Z. T.; Tang, Y. D.; Jiang, Y. S.; Bhadra, S.; Du, Y.; Ellington, A. D.; Li, B. L. *Sci. Rep.* **2016**, *6*, 36605.
(43) Xiong, E. H.; Zhen, D. S.; Jiang, L. *Chem. Commun.* **2018**, *54*, 12594−12597.
(44) Bi, S.; Yue, S. Z.; Wu, Q.; Ye, J. Y. *Chem. Commun.* **2016**, *52*, 5455−5458.
(45) Xiong, E. H.; Yan, X. X.; Zhang, X. H.; Li, Y. M.; Yang, R. Y.; Meng, L. X.; Chen, J. H. *Analyst* **2018**, *143*, 2799−2806.
(46) Carroll, A. R.; Buchanan, M. S.; Edser, A.; Hyde, E.; Simpson, M.; Quinn, R. J. *J. Nat. Prod.* **2004**, *67*, 1291−1294.

DOI: 10.1021/acs.analchem.9b04987
Anal. Chem. 2019, 91, 15317−15324

(47) Wang, S.; Bi, S.; Wang, Z. H.; Xia, J. F.; Zhang, F. F.; Yang, M.; Gui, R. J.; Li, Y. H.; Xia, Y. Z. *Chem. Commun.* **2015**, *51*, 7927−7930.
(48) Wei, L. M.; Wang, X. Y.; Wu, D.; Li, C.; Yin, Y. M.; Li, G. X. *Chem. Commun.* **2016**, *52*, 5633−5636.
(49) Huang, Y.; Zheng, J.; Wang, L.; Duan, X. G.; Wang, Y. S.; Xiang, Y.; Li, G. X. *Biosens. Bioelectron.* **2019**, *127*, 45−49.

DOI: 10.1021/acs.analchem.9b04987
Anal. Chem. 2019, 91, 15317−15324